Journal of Power Sources 256 (2014) 430–439

Contents lists available at ScienceDirect

Journal of Power Sources

journal homepage: www.elsevier.com/locate/jpowsour

Impact of the flame retardant additive triphenyl phosphate (TPP) on the performance of graphite/$LiFePO_4$ cells in high power applications

Katarzyna Ciosek Högström [a,*], Henrik Lundgren [b], Susanne Wilken [c], Tommy G. Zavalis [b], Mårten Behm [b], Kristina Edström [a], Per Jacobsson [c], Patrik Johansson [c], Göran Lindbergh [b]

[a] Department of Chemistry – Ångström Laboratory, Uppsala University, SE-751 21 Uppsala, Sweden
[b] Applied Electrochemistry, KTH Royal Institute of Technology, SE-100 44 Stockholm, Sweden
[c] Department of Applied Physics, Chalmers University of Technology, SE-412 96 Göteborg, Sweden

HIGHLIGHTS

- TPP affects the Li^+ solvation, increases the viscosity and decreases the conductivity.
- Higher amounts of TPP increase instantaneous and time-dependent polarization.
- TPP influences the interface chemistry of the $LiFePO_4$ and the graphite electrodes.
- TPP is not considered to be a suitable flame retardant for high power applications.

ARTICLE INFO

Article history:
Received 23 December 2013
Accepted 3 January 2014
Available online 23 January 2014

Dedication: Professor Per Jacobsson in memoriam.

Keywords:
Triphenyl phosphate (TPP)
Flame retardant additive
Graphite/$LiFePO_4$ cell
Electrolyte characterization
Hybrid Pulse Power Characterization (HPPC)
Electrode/electrolyte interface

ABSTRACT

This study presents an extensive characterization of a standard Li-ion battery (LiB) electrolyte containing different concentrations of the flame retardant triphenyl phosphate (TPP) in the context of high power applications. Electrolyte characterization shows only a minor decrease in the electrolyte flammability for low TPP concentrations. The addition of TPP to the electrolyte leads to increased viscosity and decreased conductivity. The solvation of the lithium ion charge carriers seem to be directly affected by the TPP addition – as evidenced by Raman spectroscopy and increased mass-transport resistivity. Graphite/$LiFePO_4$ full cell tests show the energy efficiency to decrease with the addition of TPP. Specifically, diffusion resistivity is observed to be the main source of increased losses. Furthermore, TPP influences the interface chemistry on both the positive and the negative electrode. Higher concentrations of TPP lead to thicker interface layers on $LiFePO_4$. Even though TPP is not electrochemically reduced on graphite, it does participate in SEI formation. TPP cannot be considered a suitable flame retardant for high power applications as there is only a minor impact of TPP on the flammability of the electrolyte for low concentrations of TPP, and a significant increase in polarization is observed for higher concentrations of TPP.

1. Introduction

The safety risks related to lithium-ion batteries (LiBs) have gained a lot of attention ever since the introduction of LiBs on the market in 1991. One of the main safety concerns is due to the employment of a highly flammable electrolyte based on organic solvents combined with a cell design aimed at maximizing the intrinsic high energy and power density. Abuse conditions, such as overcharge, overheating, or short circuit can lead to exothermic reactions, and in worst case thermal runaway and fire. These are all reasons contributing to the slow implementation of LiBs to the market of hybrid and electric vehicles [1–3].

Because of the above mentioned safety issues, development of electrolytes with reduced flammability has recently become a major focus – for example with the use of flame retarding additives [4,5]. Trimethyl phosphate (TMP) was one of the first investigated flame retardants [6]. However, TMP has been observed to be reduced on the surface of the negative electrode which leads to capacity fading [6–8]. Xu et al., showed that a viable path is turning to partially fluorinated alkyl as such compounds both are more effective flame retardants and have improved stability at low potentials [9–11]. Longer alkyl groups or replacement of alkyl groups with aryl substituents has also been shown to increase the

* Corresponding author. Department of Chemistry – Ångström Laboratory, Box 538, SE-751 21 Uppsala, Sweden. Tel.: +46 18 4713701; fax: +46 18 513548.
E-mail address: katarzyna.ciosek@kemi.uu.se (K. Ciosek Högström).

0378-7753/$ – see front matter © 2014 Elsevier B.V. All rights reserved.
http://dx.doi.org/10.1016/j.jpowsour.2014.01.022

electrochemical stability and flammability behavior of phosphate based flame retardants [8,12,13].

Triphenyl phosphate [13,14] (TPP or more correctly TPPa [15]) is an example of an alkyl phosphate in which the alkyl groups have been replaced with phenyl substituents. The additive provides a flame retarding effect by scavenging hydrogen radicals in the flame, prohibiting chain reactions and flame propagation [6,16], as well as forming a char layer suffocating the flame [17]. There are several studies on how TPP affects the electrochemical performance of LiBs [13,17–23]. For instance Hyung et al. and Shim et al. showed that low concentrations of TPP have little influence on the discharge capacity as well as the full cell impedance of a battery [13,21,22]. The effect of the additive on the cycling performance was later shown to be dependent on cell chemistry [23]. This was further investigated with lithium metal half-cell studies by Dahn et al., showing that an electrolyte with >20 vol% TPP led to unacceptable impedance increases for all positive electrodes [20] and that the capacity for negative electrodes decreased with increasing TPP content [19]. They attributed this capacity loss to TPP influencing the solid electrolyte interphase (SEI) leading to increased impedance. This was also suggested by Dunn et al. stating that the SEI limits the lithium intercalation kinetics, but also outlined the possibility of a change in the solvation/de-solvation of the lithium-ions [17].

The main focus of all previous studies related to TPP as an electrolyte additive has been on its effect on discharge capacity, and the studies have been limited to low [17,19,20] or intermediate currents [13,21,22]. The electrochemical performance of the electrolyte itself has not been widely studied; the only published data is the ionic conductivity at a single TPP concentration [17]. Furthermore, no studies have addressed how TPP influences the electrode/electrolyte interface.

In the present work we provide a deeper mechanistic study of the role of TTP for cycling a LiB. We do this based on an extensive characterization of a standard LiB electrolyte containing different amounts of TPP, including flammability behavior, physico-chemical properties, electrochemical stability, and high power performance in graphite/$LiFePO_4$ cells, as well as the influence on the electrode/electrolyte interface for $LiFePO_4$ positive and graphite negative electrodes. The ultimate aim is to determine whether or not TPP is a suitable flame retardant for LiBs intended for high power demanding applications, such as hybrid electric vehicles.

2. Experimental

The baseline of this study was the standard electrolyte composed of 1 M $LiPF_6$ in ethylene carbonate (EC):diethyl carbonate (DEC) in a 1:1 weight ratio (LP40, BASF, battery grade). To this electrolyte different amounts of TPP (≥99%, Sigma–Aldrich) were added to obtain electrolytes with 0–15 wt% TPP (safety tests were made with up to 20 wt% TPP). By the addition of TPP to the electrolyte the lithium salt concentration decreased, finally reaching 0.89 M at 15 wt% TPP. In order to address this secondary effect, *i.e.* the role of lowered salt concentration, a model electrolyte was prepared with no TPP, but with 0.89 M $LiPF_6$ (Sigma–Aldrich, battery grade) in EC:DEC (1:1) (Novolyte, battery grade). In order to further address the role of TPP as a possible solvent for Li^+ explicitly, a sub-set of two additional electrolytes was prepared with: i) 0.05 M $LiPF_6$ in TPP and ii) 0.15 M $LiPF_6$ in TPP.

2.1. Electrolyte characterization

Basic electrolyte characterization included the flammability behavior, various physical properties such as ionic conductivity, viscosity, and density, as well as the changes in lithium-ion solvation. The mass-transport resistivity was examined in a symmetrical Li/Li cell.

2.1.1. Flammability behavior

The flammability behavior was evaluated by both flash point (FP) and self-extinguishing time (SET) experiments. The FP is reported in centigrades (°C) and was obtained using a Petrotest ABA 4 equipment with tests performed according to the Abel method [24,25]. A few ml of electrolyte was heated continuously and an igniter was applied in the vapor phase above the liquid. The FP reported is the lowest temperature at which application of the igniter causes the electrolyte vapor to ignite. For the SET approximately 0.5 g of electrolyte was placed on a watch glass and exposed to a burner for 3 s to allow ignition. The time required for the flame to self-extinguish was recorded and normalized against the electrolyte mass. The measurements were repeated 6 times per sample and the averages are reported as the SET [26].

2.1.2. Ionic conductivity, viscosity, and density

Conductivity measurements were performed inside an argon-filled glovebox (≤1 ppm H_2O, ≤3 ppm O_2), using a Consort K912 conductometer with a SK21T micro-electrode probe. The conductometer was calibrated outside the glovebox using KCl standard solutions. The temperature dependent density and viscosity of the electrolytes were measured by inserting a few ml of sample into an Anton Paar DMA 4500/LOVIS 2000. The density was determined using an oscillating U-tube while simultaneously determining the dynamic viscosity through the falling sphere method. The values reported here were obtained at 25 °C.

2.1.3. Electrolyte mass-transport resistivity

A rewritten form of Ohm's law is used to analyze the mass-transport resistivity, which is made up of two contributions causing polarization: ohmic and diffusion resistivity [27,28]. The equation is given as

$$-\frac{(\partial\phi/\partial x)_{S.S.}}{i} = \frac{1}{\sigma} + \frac{\Delta\phi_{diff,S.S.}}{l}\frac{1}{i}\cdot\varepsilon^{\beta} \quad (1)$$

where ϕ is the electrolyte potential measured with a lithium metal reference, i the current density, σ the ionic conductivity, ε the volume fraction of electrolyte (i.e. the porosity of the separator used in the experiments), β the Bruggeman coefficient related to the tortuosity of the separator, and $\Delta\phi_{diff,S.S.}$ is the potential drop at steady-state caused by a concentration gradient in a cell of length l, polarized by a current i.

The diffusion resistivity is relatively easily extracted from a galvanostatic polarization experiment [28], here performed in an argon-filled glovebox (≤1 ppm H_2O, ≤3 ppm O_2) using a symmetrical Li/Li cell with a 500 μm thick and 6 mm inner diameter Teflon spacer ring. A specified volume of electrolyte was soaked in a Whatman GF/A glass micro fiber filter as separator, with a porosity of 0.9 and an experimentally determined Bruggeman coefficient of 3.44 [29], used for correction terms in the evaluation of the diffusion resistivity. The diffusion potential is defined as the potential between the electrodes when the galvanostatic load used to polarize the cell to steady state is interrupted. The polarization time-dependency of the diffusion potential was studied by measuring the potential during current interruptions, very short compared to the total polarization time, in order to allow concentration gradients to build up. The magnitudes of the polarization currents were chosen so that the diffusion potential right after current interruption was between 5 mV and 50 mV, to minimize noise and to avoid dendrite formation, respectively.

2.1.4. Raman spectroscopy

Samples for the Raman spectroscopy measurements were prepared by filling the electrolytes into glass vials, sealed under argon atmosphere. For each sample room temperature Raman spectra were obtained using a Bruker MultiRAM equipment with a 1064 nm Nd:YAG laser source, for an average of 2000 scans and using a spectral resolution of 2 cm^{-1}.

To support the assignment of the Raman spectra obtained experimentally in terms of vibrational modes, DFT calculations on TPP and a $[Li(TPP)]^+$ complex were performed in Gaussian 03 [30]. As a starting structure a TPP molecule was created and optimized with the B3LYP functional [31–33] and the 6-311 + G* basis set [34–36] to obtain the minimum energy structure. In order to find the preferred solvated Li^+ structure by TPP, a Li^+-ion was placed at different sites of the TPP molecule prior to geometry optimization – with the unique result of Li^+-coordination by the double bonded oxygen of the P=O group. By computing the second and partial third derivatives of the energy with respect to the vibrational modes for the optimized structures the IR and Raman spectral data; vibrational frequencies, IR intensities, and Raman activities were obtained.

2.2. Full cell tests

Galvanostatic cycling was performed on graphite/$LiFePO_4$ pouch cells (vacuum-sealed polymer-coated aluminum bags). The positive and negative electrode materials were supplied by Quallion LLC and the cells were balanced as shown in Table 1. A high resolution scanning electron microscope (SEM, Zeiss LEO 1550) was used to characterize the structure of uncycled electrode materials (see Fig. 1). The $LiFePO_4$ positive electrode has a relatively uniform distribution of nano-sized particles and the graphite negative electrode has a particle size distribution ranging from ~200 nm to a few μm. All the cell components were dried overnight in a vacuum furnace and assembled inside the argon filled glovebox. The cells were cycled galvanostatically at a low rate (C/10, 0.88 A m^{-2}) for four formation cycles between 2.5 V and 3.8 V. Subsequently, the cells were subject to an EUCAR Hybrid Pulse Power Characterization (HPPC) test cycle (120 s, Δstate-of-charge (ΔSOC) 5%, maximum C rate: 10C) [37]. Prior to the EUCAR cycle the cells were discharged to 60% SOC at a C/10 rate.

2.3. XPS electrode/electrolyte interface characterization

In order to perform the XPS electrode/electrolyte interface characterization an accelerated cycling of the cells was performed prior to any measurements. The cycling procedure described in 2.2 was followed by five more EUCAR cycles and two ISO cycles (300 s, ΔSOC 5%, maximum C rate: 20C) [38]. Between the HPPC tests two C/10 cycles were included in order to determine the capacity of the cells which was used for re-calculating C-rates for the following cycles. Prior to each test the cells were discharged to 60% SOC at a C/10 rate (determined from the last discharge capacity).

The cells were all opened in the argon filled glovebox and transferred to the XPS intro-chamber in a specially built transfer cup in order to avoid any exposure to air [39]. The XPS measurements were performed with a Perkin Elmer PHI 5500 system using monochromatized 1486.6 eV Al Kα radiation. The electron take-off angle was 45° defined relative to the surface plane of the sample. In order to avoid radiation damage the measurement time was kept as short as possible, while still discerning the shape of a spectrum. The spectra were energy calibrated using the lowest binding energy C1s core level feature set to 284.4 eV.

The relative intensities of the different features were determined using the detected core level peak areas and the Scofield theoretical photoionization cross sections [40,41]. In the presented XPS spectra the profiles were normalized to show the relative intensities of the different compounds. Iron and lithium were excluded from the quantitative analysis of the $LiFePO_4$ electrode due to an overlap of the Fe2p core level peak with the fluorine plasmon, as well as an overlap between Fe3p and Li1s core levels.

Table 1
Cell material specifications.

Negative	90 wt% MCMB graphite (Quallion LLC)
	3.8 mg cm^{-2} loading density
	Thickness 30 μm, Ø 20 mm
	Copper current collector
Positive	84 wt% $LiFePO_4$ (Quallion LLC)
	8 mg cm^{-2} loading density
	Thickness 35 μm, Ø 19 mm
	Aluminum current collector
Separator	Celgard 2320 (PP/PE/PP)
	Thickness 20 μm
Electrolyte	1 M $LiPF_6$ in EC:DEC 1:1 by weight
	(LP40, BASF) + 0–15 wt% TPP (Sigma–Aldrich)

3. Results and discussion

The goal of this study is to relate the properties of electrolytes containing TPP to full cell cycling in a high power LiB context. The study is divided into three parts: i) electrolyte characterization via studying the flammability behavior, viscosity, density, conductivity, and mass-transport resistivity, ii) full cell tests in graphite/$LiFePO_4$ cells, focusing on high power performance through HPPC tests, and finally iii) XPS electrode/electrolyte interface characterization.

3.1. Electrolyte characterization

The characteristics of the ubiquitous battery solvents EC and DEC as such are well known and can readily be found in data sheets describing properties such as viscosity and density *etc*. When it comes to employing TPP as an additive to EC:DEC based electrolytes, however, the resulting properties are still to be elucidated, why we perform both basic (performance) characterization as well as safety oriented tests.

3.1.1. Flammability behavior

The flammability behavior is here evaluated by two different measures: a flammability test – aiming to determine the likeliness of ignition, and an SET test – more aiming at describing the consequences of such an event. The flammability tests summarized in Table 2 reveal the flash point (FP) to change only slightly from 36.0 °C for the standard electrolyte to 37.9 °C for a full 20 wt % TPP (Table 2). This was, however, to be expected as the FP mainly is dependent on the amount of highly flammable organic solvents, and considering that even an addition of 15 wt% TPP results in an electrolyte composition of 95 mol% EC:DEC and only 5 mol% TPP. Thus, TPP does not alter the vapor phase composition ignited, which is in agreement with previously published results [8].

Turning to the self-extinguishing times (SETs) in Table 2, a significant reduction by 12 s or 19% can be observed (the SET changes from 62 s g^{-1} for the standard electrolyte to 50 s g^{-1} upon addition of 15 wt% TPP). In the literature we find a single reference to SET measurements for TPP; Dunn et al. reported a reduction by 61% upon addition of 15 wt% TPP to 1 M $LiPF_6$ EC:EMC (3:7) [17], and "retarded electrolyte" behavior (6 s g^{-1} <SET> 20 s g^{-1} [8]). The discrepancy with our findings is likely caused both by the use of a different carbonate solvent as well as a different experimental

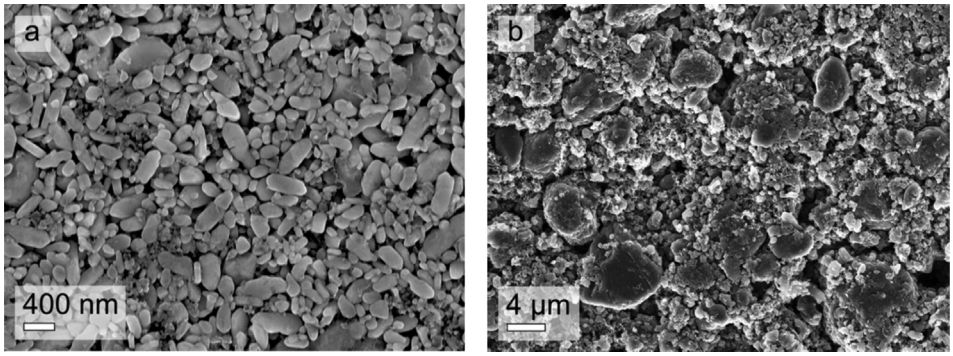

Fig. 1. SEM images of a) $LiFePO_4$ positive electrode and b) graphite negative electrode.

protocol – an experimental set-up standard is lacking in the field. For additives similar to TPP and approximately 15 wt%, the SET changes can be up to 72% as found for tris-(2,2,2-trifluoroethyl) phosphate (TFP) and bis(2,2,2-trifluoroethyl)-methylphosphate (BMP), or 45% for trimethyl phosphate (TMP), triethyl phosphate (TEP) and hexamethoxycyclotriphosphazene (HMPN) [8,9]. These studies were all performed with 1 m $LiPF_6$ in EC/EMC and another experimental protocol than ours. Lombardo et al. performed SET tests with the same procedure as ours [42] and for an addition of 30 wt% of the ionic liquid *N*-butyl-*N*-methylpyrrolidinium bis(trifluoromethanesulfonyl)imide ($Pyr_{14}TFSI$) to an EC:DMC electrolyte obtained 21% SET reduction. This indicates that our 19% SET reduction for 15 wt% TPP is reasonable.

3.1.2. Ionic conductivity, viscosity, and density

In Fig. 2 we have compiled the data on ionic conductivity (σ), dynamic viscosity (η) and the Walden product, all as functions of electrolyte TPP content. The ionic conductivity decreases with addition of TPP; from 7.9 mS cm^{-1} for the standard electrolyte to 5.9 mS cm^{-1} for 15 wt% TPP. To check for the possible influence of the decreased salt concentration upon TPP addition, a reference measurement on an electrolyte without TPP but with the same salt concentration (0.89 M) was made; resulting in exactly the same value (7.9 mS cm^{-1}), thus the conductivity decrease upon TPP addition cannot be due to the lowered salt concentration.

The standard electrolyte has a density of 1.222 g cm^{-3} (not shown) and a dynamic viscosity of 4.492 mPa s. With the addition of TPP both increase, finally reaching 1.224 g cm^{-3} and 5.391 mPa s for 15 wt% TPP.

According to the Walden rule, the product of the limiting molar conductivity $\Lambda = \sigma/c_{Li}$ and the solvent's viscosity $k = \Lambda^*\eta$ should be constant for infinitely diluted electrolyte solutions at a fixed temperature [43]. In this case, the ion mobility is purely governed by the ion migration given by the diffusion according to the Stokes–Einstein equation [44]. Here the Walden product is almost constant with TPP addition, and thus the observed decrease in conductivity is mainly due to the increasing viscosity, as expected.

Table 2
Flashpoints (FPs) and self-extinguishing times (SETs) for different electrolyte compositions. The FP of the 15 wt% TPP containing electrolyte can be extrapolated to be approx. 37.4 °C.

Electrolyte composition/wt% TPP	Flashpoint/°C (±0.7)	Self-extinguishing time/s g^{-1}
0	36.0	62.0 (±5)
1	36.9	61.5 (±2)
3	36.4	58.0 (±4)
5	37.4	59.0 (±7)
10	37.0	51.5 (±5)
15	–	50.5 (±6)
20	37.9	40.0 (±4)

3.1.3. Electrolyte mass-transport resistivity

Measurements of the ohmic and diffusion resistivities, as described by Equation (1), were undertaken and the results are shown in Fig. 3. The diffusion resistivity linked to the development of salt concentration gradients in the cell during polarization is always significantly larger than the ohmic resistivity (the inverse of the conductivity shown in Fig. 2), independent of TPP content. Both resistivities increase with TPP content; the ohmic resistivity increases approximately linearly with TPP content, while the diffusion resistivity does not increase further after ca. 10 wt% TPP. The increase in diffusion resistivity (68%) is roughly twice the increase in ohmic resistivity (35%), suggesting that the transport rate of lithium ions is more affected than the transport rate of anions by the addition of TPP.

In Fig. 4 we show the time-dependent diffusion resistance for the standard electrolyte and with 15 wt% TPP. Steady-state is reached after ~7 and ~15 min, respectively, and the diffusion polarization is always larger than the ohmic polarization. The relatively long times to reach steady-state is due to the quite thick cells (500 μm) used; reducing the thickness by an order of magnitude, thus coming closer to commercial cells, would reduce the time to reach steady-state by two orders of magnitude. That the time needed to reach steady-state is more than doubled for the electrolyte containing TPP suggests mainly a slower salt diffusion to cause the increased diffusion resistivity, since the time constant for diffusion is directly proportional to the diffusion coefficient (as follows from Fick's second law).

3.1.4. Raman spectroscopy

In order to uniquely address any molecular interaction changes occurring upon TPP addition Raman spectroscopy was performed on the standard electrolyte, the neat TPP, as well as the TPP containing electrolytes. The standard electrolyte data contain signatures of PF_6^-, EC, and DEC, for which all modes can be assigned using the literature [45–47]. As both carbonate solvents participate in the lithium-ion solvation, also the Li^+-coordinated solvent, shifted, modes can be observed for EC as well as DEC [47,48]. The Raman features obtained for neat TPP can be assigned to vibrational modes with the help of DFT calculations. Nishikawa et al. [49] have previously reported the computational and experimental IR frequencies between 1000 and 1600 cm^{-1} using B3LYP/6-31G(d), which for reasons of completeness we here report for the whole range 400–3200 cm^{-1} using B3LYP/6-311 + G* (Table S1). A table of both experimental and computed frequencies, and IR intensities

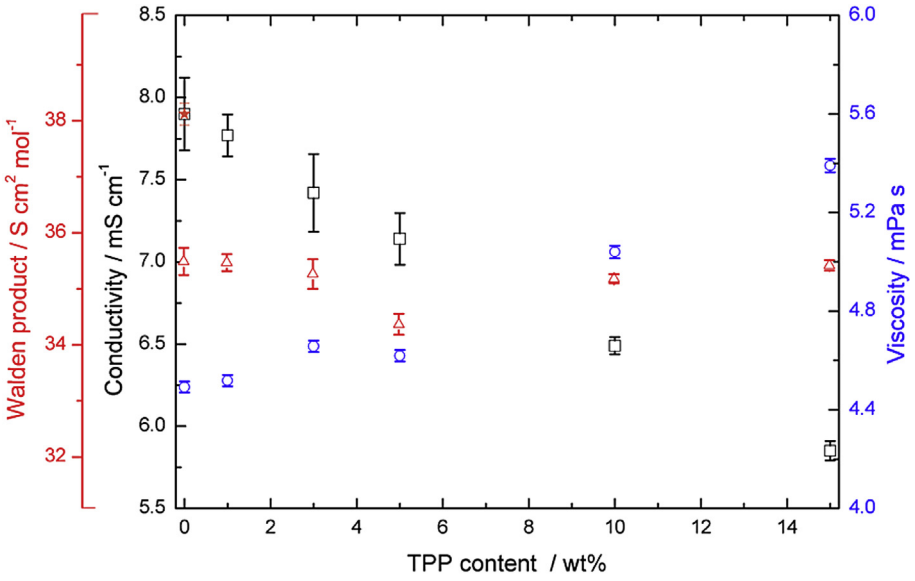

Fig. 2. Physical characterization of the electrolytes at 25 °C: conductivity (black squares), viscosity (blue circles) and the Walden product (red triangles). The red star denotes the conductivity for the 0.89 M $LiPF_6$ 0 wt% TPP electrolyte. (For interpretation of the references to colour in this figure legend, the reader is referred to the web version of this article.)

including mode assignments for TPP, are all to be found in the Supplementary information S1.

In Fig. 5 we show that upon addition of TPP a gradual increase in intensity of new bands is detected, while EC:DEC associated modes gradually decrease. The strongest features are observed at 616, 1006, and 1592 cm^{-1}, while the other new signals are partly overlapping with those of the standard electrolyte. A comparison to the spectral features of the neat TPP shows good agreement except for the signal at 932 cm^{-1}, which we find shifted to 945 cm^{-1} (Table 3). In order to determine if this shift is due to the different molecular environment of TPP in the electrolyte or if it is the indication of a new interaction, e.g. lithium-ion affected, we calculated the frequencies and Raman activities of TPP and $[Li(TPP)]^+$ (Table 3). The predicted Li^+ induced shifts are from a few up to 26 wavenumbers, and at least the latter should be detectable under realistic experimental conditions. The largest $\Delta\nu$, for a vibrational mode composed of ring breathing and ν_s(P–O) for neat TPP at 928 cm^{-1}, with an additional $\nu_{as}(Li^+–O)$ internal coordinate contribution for the $[Li(TPP)]^+$ at 954 cm^{-1}, is indeed found in this region. Even at as low concentrations as 1 wt% TPP, however, we only detect one broad feature at 954 cm^{-1}. In order to probe directly for the possible lithium-ion effect, the Raman spectra of the 0.05 M and 0.15 M $LiPF_6$ in TPP electrolytes were compared (Fig. 6). In the spectral region of 925–950 cm^{-1} we observe a gradual transition from the free TPP band to the lithium-ion affected band upon addition of $LiPF_6$, a clear signature and evidence of a direct interaction between TPP and lithium-ions. Furthermore, the absence of the free TPP mode in the TPP containing electrolytes indicates that in those, all TPP molecules are lithium-ion coordinated. The other large predicted shift of the free ring bending and ν_s(P–O) mode at 713 cm^{-1} toward the lithium-ion affected mode at 733 cm^{-1} (including $\nu_s(Li^+–O)$) is overlapped strongly by the $\delta(C{=}O_{ring})$ EC mode in the LP40 and TPP containing electrolytes. Analysis of the carbonate solvent free spectra shows the same transition of both modes, free and solvated at 728 and 720 cm^{-1}, respectively (not shown). Therefore, we conclude that TPP directly participates in the lithium-ion coordination, and is even strongly preferred compared to EC and DEC as we cannot detect any signature of free TPP in the TPP:EC:DEC electrolytes. This is in agreement with Dunn et al., who have previously suggested that TPP may influence the solvation and

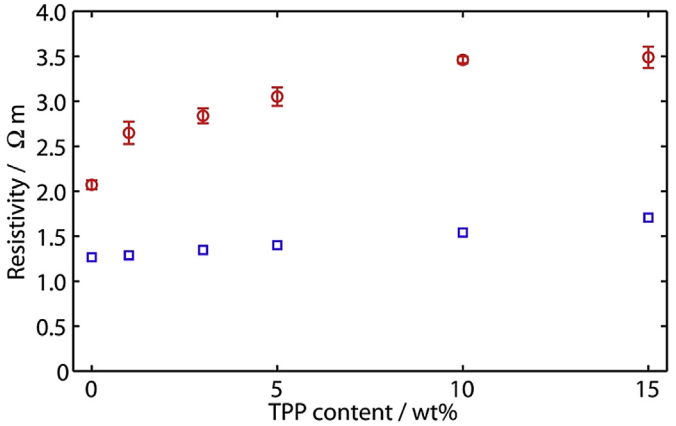

Fig. 3. The diffusion (○) and ohmic (□) resistivities for different TPP contents (measured at steady-state).

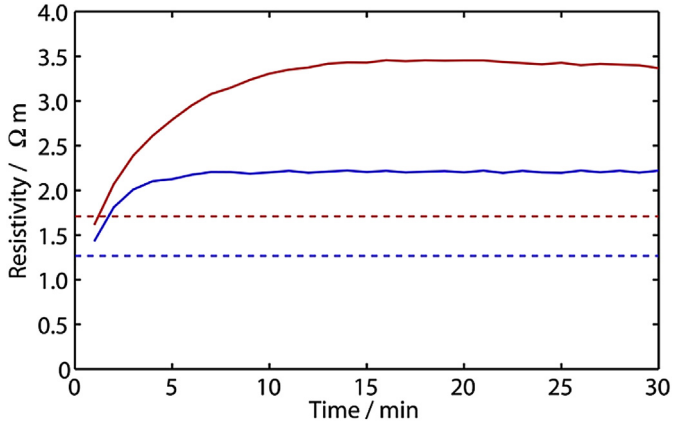

Fig. 4. The evolution of the time-dependent diffusion resistance for the standard electrolyte (blue) and with the addition of 15 wt% TPP (red). The time-independent ohmic resistance is shown as dashed lines. (For interpretation of the references to colour in this figure legend, the reader is referred to the web version of this article.)

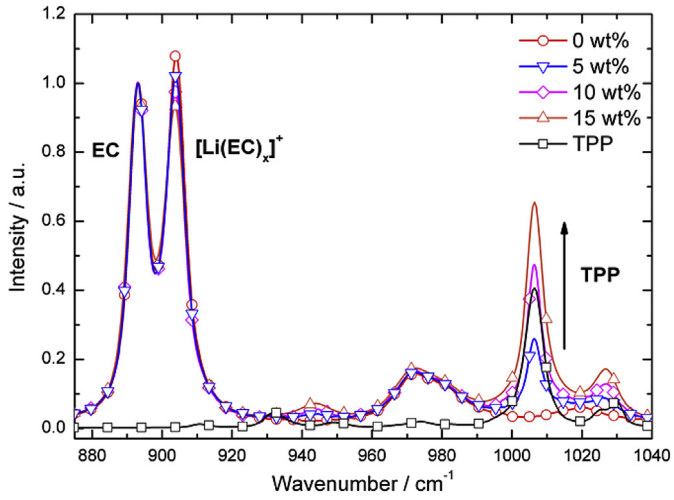

Fig. 5. Raman spectra as a function of wt% TPP addition: 0 (○), 5 (Δ), 10 (◇), and 15 (▽), respectively. The (□) denotes the spectrum of pure TPP. All spectra normalized using the amplitude of the ring breathing mode of EC at 893 cm^{-1}.

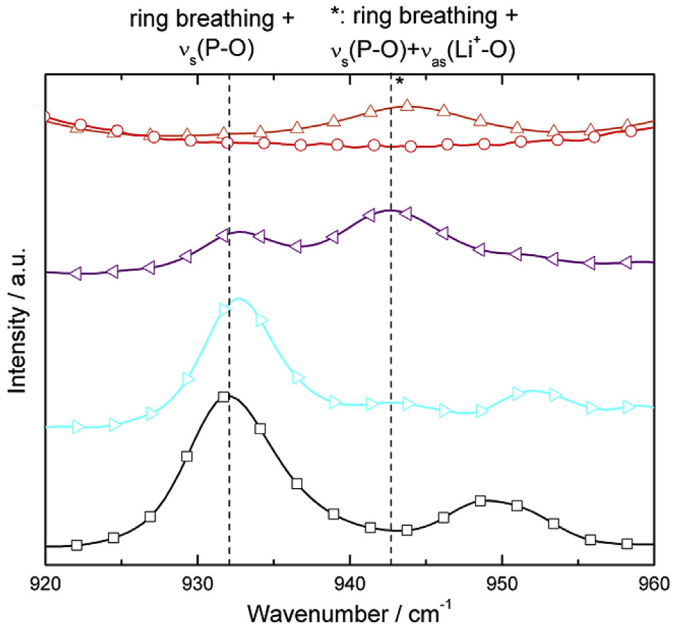

Fig. 6. Raman spectra as a function of $LiPF_6$ concentration in TPP: 0 (□), 0.05 M (), 0.15 M (◁), respectively. The (○) and (Δ) denote the spectra of pure LP40 and LP40 + 15 wt% TPP, respectively. The lines mark the modes associated to the ring breathing and ν_s(P–O) of neat TPP, and the additional contribution of $\nu_s(Li^+–O)$ in the $[Li(TPP)]^+$ (*).

coordination of the lithium-ions, and furthermore, influence the de-solvation characteristics [17].

Consequently, the carbonate solvent – lithium-ion interaction upon TPP addition must change and serves as an indirect additional check, and therefore we turned to other regions affected by Li^+-coordination. The $\delta(C{=}O_{ring})$ mode of EC at 717 cm^{-1} is shifted to 729 cm^{-1} upon Li^+-coordination [46], but as addressed earlier, is strongly overlapping with the P–O ring mode of TPP at 726 cm^{-1} and therefore difficult to evaluate. Fortunately, the EC ring breathing mode at 893 cm^{-1}, shifted 11 cm^{-1} to 904 cm^{-1} upon Li^+-coordination [48], are both clearly visible and can be analyzed in detail (not shown, but note that the latter overlaps with the $\nu(CH_2–O)$ mode of both free and Li^+-coordinated DEC). In order to separate each band, careful peak fitting using Voigt profiles was performed using both the literature value for the coordinated DEC band position, and the relaxed peak position at 911 cm^{-1} [47] and 909 cm^{-1}, respectively. The amplitudes as well as the peak shapes of the four peaks change with additive content, while the integration results in a nearly constant ratio of free solvent to Li^+-coordinated peaks – independent of additive content. Based on the lithium salt concentration (1.00–0.89 M), we find the apparent cation solvation numbers to be decreasing for both fitting routines (Supplementary information S2). Hence, both by the direct TPP observations and by the indirect EC:DEC studies, we find that the direct Li^+ solvation in EC:DEC changes upon TPP addition.

The addition of TPP also affects the physico-chemical properties as shown by electrolyte characterization (density, viscosity, conductivity, FP), and the observed changes are comparable to those of other implemented flame retardants [50,51]. Ding et al. [52] associate the conductivity drop with addition of their flame retardant TFP to its low dielectric constant and a suppression of salt dissociation. We can only speculate that this effect can contribute here as well, since according to our DFT calculations TPP has a dipole moment of 3 Debye and our observation of $LiPF_6$ being only weakly soluble in pure TPP.

Table 3
Experimental frequencies (pure TPP, LP40 electrolyte with *x* wt% TPP), computed frequencies and relative Raman activities, and mode assignments.

Experimental (TPP) (LP40 + *x* wt% TPP)		Computed (TPP)		Computed $[Li(TPP)]^+$		Mode assignment
ν_{exp}/cm^{-1}	ν_{exp}/cm^{-1}	ν_{calc}/cm^{-1}	Relative Raman activity/a.u.	ν_{calc}/cm^{-1}	Relative Raman activity/a.u.	
598		567	0.032	577	0.055	Ring bending + δ(O–P–O) (+$\delta(Li^+–O–P)$)
616	616	629	0.053	626	0.055	Ring bending (+$\delta(Li^+–O–P)$)
				653	0.070	Ring bending (+$\delta(Li^+–O–P)$)
726	Overlapped	713	0.274	733	0.181	Ring bending + ν_s(P–O) + ($\nu_s(Li^+–O)$)
790		782	0.067	798	0.115	Ring bending + δ_{as}(O–P–O) (+$\delta_s(Li^+–P–O)$)
932	945	928	0.075	954	0.107	Ring breathing + ν_s(P–O) (+$\nu_{as}(Li^+–O)$)
1006	1006	1020	1.000	1020	1.000	ν_s(ring)
1025		1048	0.083	1046	0.208	δ(C–H)
1030	1027	1049	0.239	1049	0.173	δ(C–H) [40]
1233	Overlapped	1246	0.738	1238	0.342	δ(C–H), ν_s(O–P–O) [49] + $\nu_{as}(Li^+–O)$
1294		1303	0.085			ν(P=O) [49]
1592	1591	1634	0.171	1631	0.229	Ring deformation [49]
1599	1601	1637	0.295	1634	0.251	Ring deformation
~3200	3077	3202	2.113	3205	5.065	ν(C–H)

ν = stretching; δ = in-plane bending; γ = out-of-plane bending; s = symmetrical; and as = asymmetrical.

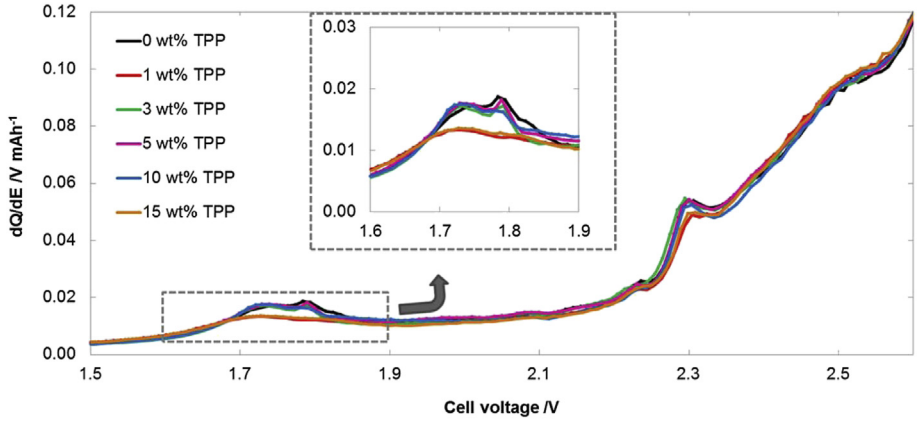

Fig. 7. The differential capacities during first charge for graphite/$LiFePO_4$ cells containing different concentrations of TPP.

3.2. Full cell tests

In order to determine the influence of TPP on LiB performance, six electrolytes with different TPP concentrations were tested in full graphite/$LiFePO_4$ cells.

In Fig. 7 we show the differential capacities for graphite/$LiFePO_4$ cells during the first charge, where the broad range between 1.5 and 2.6 V is shown in order to determine if TPP is being reduced or not on the negative electrode. Clearly, there are no extra peaks observed for electrolytes containing TPP compared to the standard electrolyte. All previous studies have shown TPP to be electrochemically stable up to 5 V, and there have been no signs of TPP reduction on the negative electrode [13,21,53]. However, Dunn et al. recently claimed TPP to be electrochemically unstable, being reduced at 1.8 V *vs.* Li^+/Li [17] at a graphite surface, which corresponds to ~1.7 V for the present graphite/$LiFePO_4$ cell. Indeed, there is a small reductive peak present at ~1.7 V in Fig. 7, but this most likely corresponds to reduction of trace oxygen in the electrolyte or oxygen surface groups [54] and therefore it is less pronounced in some of the cells (1 and 15 wt% TPP). In addition, the peak is clearly seen for the standard electrolyte and therefore cannot possibly correspond to any TPP reduction.

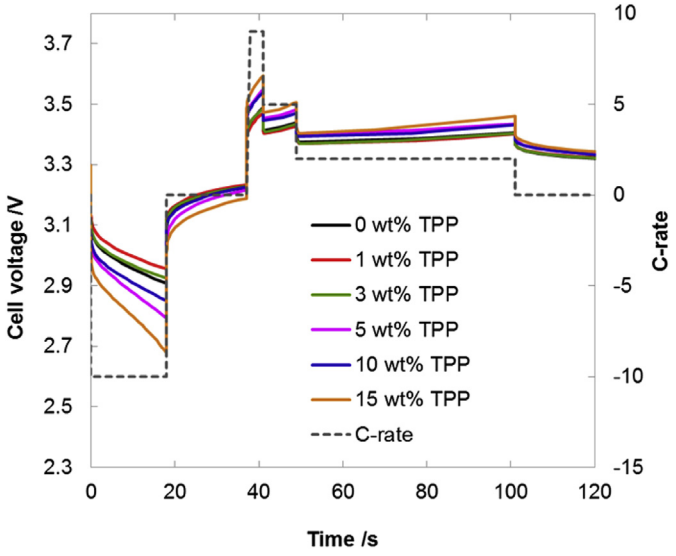

Fig. 8. Cell voltages and C-rates for EUCAR test cycles of graphite/$LiFePO_4$ cells with different TPP concentrations.

The impact of TPP on the high power performance for graphite/$LiFePO_4$ cells was investigated with EUCAR tests [37]. In Fig. 8 we show the EUCAR cycle for cells with different TPP contents and in Table 4 the calculated changes in energy efficiency during this cycle, with the energy efficiency of the standard electrolyte as a reference, are given. The latter shows that increasing concentrations of TPP lead to significant decreases in energy efficiency, which is due to the increased polarization, seen as larger voltage responses in Fig. 8.

Furthermore, the shape of the responses varies, which indicates that the contributions to the total polarization differ. The polarization during the pulse can roughly be divided into two contributing parts: instantaneous and time-dependent. The former is mainly due to contact resistance between different phases and materials, activation of the electrochemical reactions, and ohmic resistivity of the electrolyte and the solid phase. The latter part is the diffusion polarization, caused by the diffusion resistivity in the electrolyte and in the solid phase [29,55].

The instantaneous and time-dependent contributions to the polarization were separated during the first 10C discharge pulse and are shown in Table 5. In Fig. 9 we show the corresponding cell voltages; the instantaneous polarization increases with higher TPP concentrations, in good agreement with the ohmic resistivity determined in Section 2.1.3. The time-dependent polarization caused by the diffusion resistance likewise increases with TPP

Table 4
Calculated changes in energy efficiency during the EUCAR tests compared to a standard electrolyte cell (energy efficiency = 87.4%).

Electrolyte composition/wt% TPP	Δ Energy efficiency/%
1	0.9
3	0.1
5	−5.0
10	−3.2
15	−7.7

Table 5
Comparison of polarizations for the 10C discharge pulse.

Electrolyte composition/wt% TPP	Instantaneous polarization/V	Time-dependent polarization/V
0	−0.096	−0.286
1	−0.082	−0.255
3	−0.106	−0.259
5	−0.111	−0.390
10	−0.138	−0.308
15	−0.139	−0.481

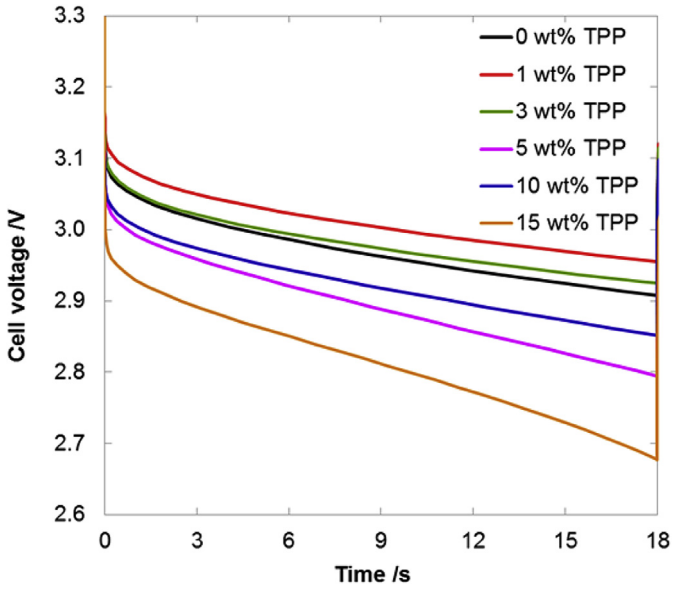

Fig. 9. Cell voltage during the first 18 s of 10C discharge in the EUCAR cycle.

concentration, also this in agreement with the diffusion resistivity determined in Section 2.1.3.

The cells with 0–3 wt% TPP have relatively similar polarizations. The variations between cells are in fact exceeding the effect of the TPP addition (Table 5). Samples with 5 and 10 wt% TPP show more pronounced decreases in performance with high increase in time-dependent polarization. For cells with 15 wt% TPP a significant decrease in performance with a high increase in instantaneous and time-dependent polarization, 46% and 68%, respectively, is observed. In a few cases, however, the variations in between cells are of the same order of magnitude as the effect of TPP addition, possibly due to variations in contact resistance. The trends above are more pronounced in later cycling data (Supplementary information S3–S5), where variations between cells have a smaller influence.

3.3. XPS electrode/electrolyte interface characterization

It is at the electrode/electrolyte interfaces, where the thermal reactions first start on the graphite side [56] and these are the interfaces layers which can lead to reduced lithium transport [1]. In order to gain insight into how TPP influences the electrode/electrolyte interfaces, positive and negative electrodes from six cells, cycled with electrolytes with different concentrations of TPP, were examined with XPS.

In Fig. 10 we present the C1s and P2p XPS spectra of unwashed and washed $LiFePO_4$ positive electrodes, respectively. The contribution from hydrocarbons (284.4 eV in C1s spectra) is growing significantly with increased TPP concentration for the unwashed electrodes for all samples. The high binding energy C1s feature at 290.2 eV, which is attributed to C–F bonds present in the binder and carbonates formed during solvent reduction [57], disappears when TPP is present in the electrolyte. Instead, a broad peak at ~290.5 eV appears. This is a shake-up peak, formed due to aromatic $\pi-\pi^*$ transitions in the phenyl groups present in TPP. When moving to the P2p spectra, the phosphate contribution (133.5 eV) assigned to the bulk material, is decreasing/disappearing for higher TPP concentrations. The XPS spectrum for $LiFePO_4$ cycled with the standard electrolyte, however, shows the expected interface layer to be thin with a large contribution from the phosphate for both unwashed and washed samples [58,59]. With increased TPP concentration a new feature, TPP* at 134.5 eV, is formed, which can be attributed to TPP itself or a compound with a very similar environment around phosphorous as in TPP.

Comparing spectra for unwashed and washed $LiFePO_4$ shows that the latter one has decreasing amounts of the feature attributed to P–F bonds (~136.3 eV) and displaying increased amounts of the phosphate contribution (133.5 eV). In spite of this, similar trends are observed for both unwashed and washed electrodes. With

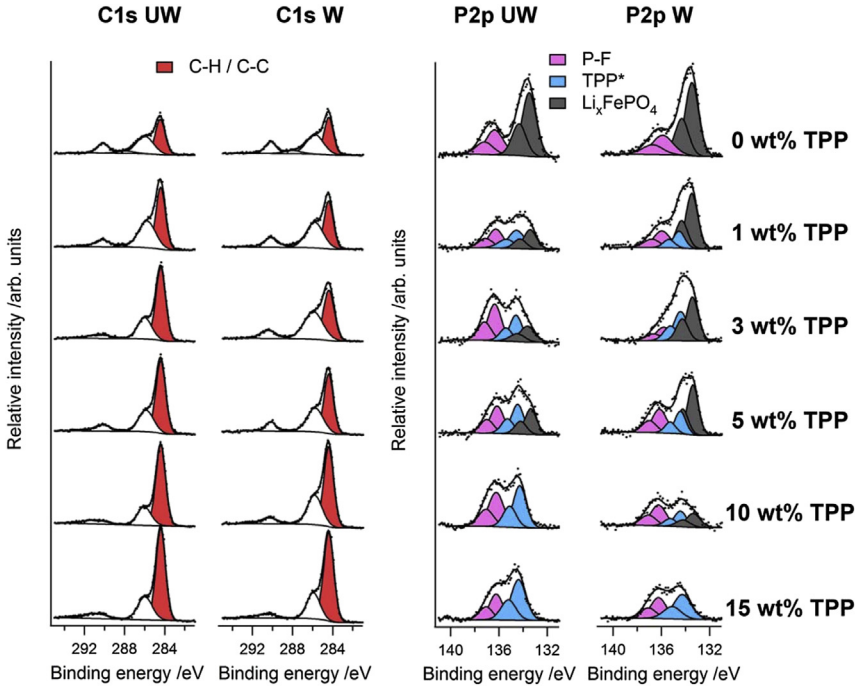

Fig. 10. C1s and P2p spectra of unwashed (UW) and washed (W) $LiFePO_4$ electrodes.

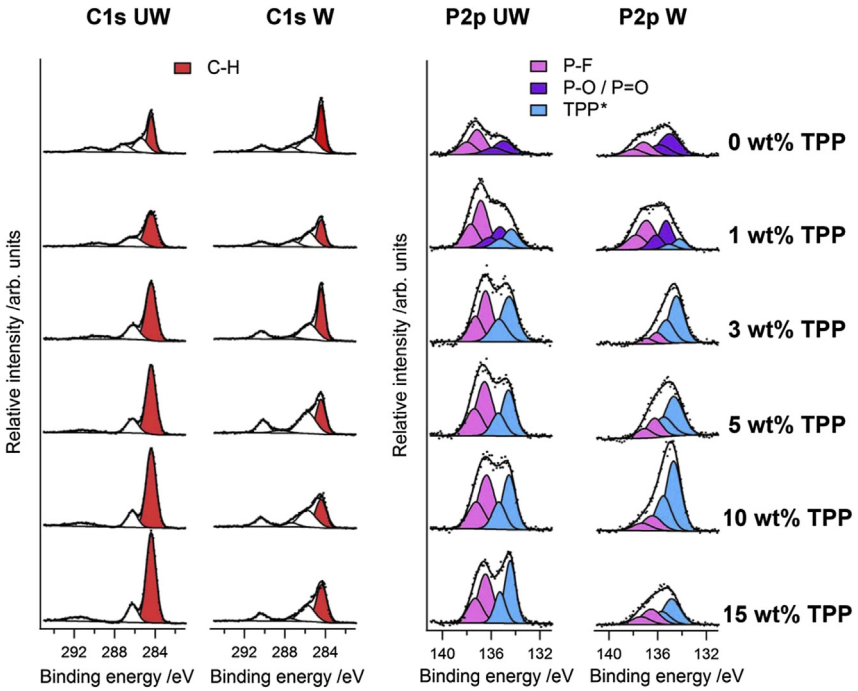

Fig. 11. C1s and P2p spectra of unwashed (UW) and washed (W) graphite electrodes.

increasing concentration of TPP the phosphate bulk material contribution is decreasing, indicating that a progressively thicker interface layer is formed on the electrode surface. At the same time the contributions from peaks assigned to TPP* are increasing.

In Fig. 11 we present the XPS spectra of unwashed and washed graphite negative electrodes. For unwashed graphite electrodes, similar trends are observed as for the $LiFePO_4$ electrodes; increasing TPP concentration leads to increased amounts of hydrocarbons (284.4 eV in the C1 spectra). At the same time the shake-up (~290.5 eV) attributed to aromatic $\pi-\pi^*$ transitions in phenyl groups is increasing. Interestingly, the C1s spectra of unwashed and washed electrodes differ significantly, more than in the case for the $LiFePO_4$ electrodes. Most of the TPP contribution to the C1s spectra seems to be washed off and a more standard SEI with respect to carbonaceous compounds: C—O (285.7 eV), COO (287.4 eV) and CO_3 (290.3 eV) features is appearing [41,57].

Moving to the P2p spectra in Fig. 11, the feature attributed to P—F bonds is decreasing after washing. With increased TPP concentration, the P—O/P═O feature is disappearing and a new feature, TPP* at 134.6 eV is appearing. As for the positive electrode, this could be attributed to TPP itself or to a compound with a similar environment around phosphorous as in TPP.

The electrode/electrolyte interface characterization shows that TPP influences the interface chemistry on both the $LiFePO_4$ positive electrode and the graphite negative electrode. Interestingly, the effects are more pronounced for unwashed samples, probably as the more viscous TPP containing electrolytes are deposited on the electrode surfaces. For the $LiFePO_4$ positive electrode there are only small changes between washed and unwashed electrodes; in both cases the electrode/electrolyte interface gets thicker for higher TPP concentrations. When the electrolyte deposit is washed away from the graphite electrode, a more standard SEI is appearing. However, even on washed graphite samples substantial amounts of TPP* features are found. Even though TPP is not reduced at the negative electrode, it participates in SEI formation. This could be due to chemical reactions with, e.g., radicals which are formed during solvent decomposition. In theory, surface film formation contributes to the polarization of a LiB in two different ways. Firstly, the film can inhibit the activation of the electrochemical reactions, since it introduces an additional resistance at the surface of the active material. Secondly, if the film becomes thick enough, it will decrease the size of the pores in the porous electrodes and thereby worsen electrolyte mass transport. Work presented previously on the same electrode materials support the fact that the latter is more significant [60]. The detected films could therefore limit the already severely impaired mass-transport properties even more.

4. Conclusions

TPP is used as a flame retarding additive in order to increase the safety of the organic electrolytes in LiB. We show, however that addition of 15 wt% TPP to the electrolyte is not effective enough to create a “non-flammable” electrolyte (a SET <6 s g^{-1} [8]).

A detailed experimental and computational vibrational analysis of the electrolytes yields direct signs of the Li^+-coordination being affected by TPP and the overall conductivity to decrease as a function of TPP concentration — and more so than for a simple viscosity related effect, as shown by the changing Walden product. This data was also confirmed by the electrolyte mass-transport resistivity measurements showing increased diffusion resistivity. Current interrupt measurements indicate that this increase is due to a decrease of the Li^+ diffusion rate, well in line with the results from the vibrational analysis.

Graphite/$LiFePO_4$ full cell tests show that higher TPP concentrations leads to higher polarization and therefore lower energy efficiency. Both the instantaneous and time-dependent polarization increases for higher TPP concentrations. It is also shown that the diffusion resistance has the highest impact on the overall cell performance.

TPP influences interface chemistry on both the $LiFePO_4$ positive electrode and the graphite negative electrode. For the positive electrode higher amounts of TPP lead to thicker interface layers. Even though TPP is not electrochemically reduced on the negative electrode, it participates in SEI formation, which could be explained

by chemical reactions e.g. with radicals formed during solvent reduction. These changes in the interface chemistry could limit the activation of the electrochemical reactions and affect the performance of the cell.

TPP is not considered to be a suitable flame retardant for high-power applications, such as hybrid electric vehicles. The low impact on flammability of the electrolyte at low concentrations competes with the significant increase in instantaneous and time-dependent polarization at higher concentrations. Therefore, it is not possible to find a balanced composition for a thermally stable electrolyte with a well performing cell behavior.

Acknowledgments

The Swedish Hybrid Vehicle Centre (SHC) is gratefully acknowledged for financing. We would also like to thank Shizhao Xiong, Chalmers, for support with the SET measurements and Dr. Mario Wachtler and Steffen Hess at ZSW, Ulm, Germany, for kindly making their FP tester available. The Chalmers Area of Advance Transport support to Patrik J is also gratefully acknowledged. The support from StandUp for Energy to MB and KE is gratefully acknowledged.

Appendix A. Supplementary data

Supplementary data related to this article can be found at http://dx.doi.org/10.1016/j.jpowsour.2014.01.022.

References

[1] K. Xu, Chem. Rev. 104 (2004) 4303.
[2] D.P. Abraham, E.P. Roth, R. Kostecki, K. McCarthy, S. MacLaren, D.H. Doughty, J. Power Sources 161 (2006) 648.
[3] R. Spotnitz, J. Franklin, J. Power Sources 113 (2003) 81.
[4] S.S. Zhang, J. Power Sources 162 (2006) 1379.
[5] S. Wilken, P. Johansson, P. Jacobsson, in: B. Scrosati, K.M. Abraham, W. van Schalkwijk, J. Hassoun (Eds.), Lithium Batteries: Advanced Technologies and Applications, John Wiley & Sons, 2013, pp. 39–70.
[6] X. Wang, E. Yasukawa, S. Kasuya, J. Electrochem. Soc. 148 (2001) A1058.
[7] X. Wang, E. Yasukawa, S. Kasuya, J. Electrochem. Soc. 148 (2001) A1066.
[8] K. Xu, M.S. Ding, S. Zhang, J.L. Allen, T.R. Jow, J. Electrochem. Soc. 149 (2002) A622.
[9] K. Xu, M.S. Ding, S. Zhang, J.L. Allen, T.R. Jow, J. Electrochem. Soc. 150 (2003) A161.
[10] K. Xu, S. Zhang, J.L. Allen, T.R. Jow, J. Electrochem. Soc. 150 (2003) A170.
[11] K. Xu, S. Zhang, J.L. Allen, T.R. Jow, J. Electrochem. Soc. 149 (2002) A1079.
[12] Q. Wang, J. Sun, X. Yao, C. Chen, Electrochem. Solid-State Lett. 8 (2005) A467.
[13] Y.E. Hyung, D.R. Vissers, K. Amine, J. Power Sources 119-121 (2003) 383.
[14] J. Green, J. Fire Sci. 10 (1992) 470.
[15] Y. Wang, Y. Xia, S. Luo, Makromol. Chem. Macromol. Symp. 74 (1993) 295.
[16] A. Granzow, Acc. Chem. Res. 11 (1978) 177.
[17] R.P. Dunn, J. Kafle, F.C. Krause, C. Hwang, B.V. Ratnakumar, M.C. Smart, B.L. Lucht, J. Electrochem. Soc. 159 (2012) A2100.
[18] X. Xia, P. Ping, J.R. Dahn, J. Electrochem. Soc. 159 (2012) A1834.
[19] X. Xia, P. Ping, J.R. Dahn, J. Electrochem. Soc. 159 (2012) A1460.
[20] P. Ping, Q.S. Wang, J.H. Sun, X. Xia, J.R. Dahn, J. Electrochem. Soc. 159 (2012) A1467.
[21] E.-G. Shim, T.-H. Nam, J.-G. Kim, H.-S. Kim, S.-I. Moon, J. Power Sources 172 (2007) 919.
[22] E.-G. Shim, T.-H. Nam, J.-G. Kim, H.-S. Kim, S.-I. Moon, J. Power Sources 172 (2007) 901.
[23] M. Smart, F. Krause, C. Hwang, W. West, ECS Trans. 35 (2011) 1.
[24] ISO/TC 28, ISO 13736:2013—Abel Closed-cup Method, 2013.
[25] V. Wierzbicki, Flash Point Test. A User's Guide, 2007. http://www.pointeclair.com/IMG/pdf/Petrotest_Flash_Point_User_s_Guide.pdf.
[26] L. Lombardo, S. Brutti, M.A. Navarra, S. Panero, P. Reale, J. Power Sources 227 (2012) 8.
[27] A. Nyman, M. Behm, G. Lindbergh, Electrochim. Acta 53 (2008) 6356.
[28] J. Lindberg, H. Lundgren, G. Lindbergh, M. Behm, J. Power Sources (2013) in press.
[29] A. Nyman, T.G. Zavalis, R. Elger, M. Behm, G. Lindbergh, J. Electrochem. Soc. 157 (2010) A1236.
[30] M.J. Frisch, G.W. Trucks, H.B. Schlegel, G.E. Scuseria, M.A. Robb, J.R. Cheeseman, Gaussian 03 Revis. D.02, 2004.
[31] A.D. Becke, J. Chem. Phys. 98 (1993) 5648.
[32] C. Lee, W. Yang, R.G. Parr, Phys. Rev. B 37 (1998) 785.
[33] S.H. Vosko, L. Wilk, M. Nusair, Can. J. Phys. 58 (1980) 1200.
[34] A.D. McLean, G.S. Chandler, J. Chem. Phys. 72 (1980) 5639.
[35] R. Krishnan, J.S. Binkley, R. Seeger, J.A. Pople, J. Chem. Phys. 72 (1980) 650.
[36] T. Clark, J. Chandrasekhar, G.W. Spitznagel, P.V.R. Schleyer, J. Comput. Chem. 4 (1983) 294.
[37] EUCAR: Traction Battery Working Group, Specification of Test Procedures for Hybrid Electric Vehicle Traction Batteries, 1998.
[38] Electrically Propelled Road Vehicles – Test Specifications for Lithium-ion Traction Battery Packs and Systems – Part 1: High-power Applications, 2011. ISO 12405–1.
[39] S. Malmgren, K. Ciosek, R. Lindblad, S. Plogmaker, J. Kühn, H. Rensmo, K. Edström, M. Hahlin, Electrochim. Acta 105 (2013) 83.
[40] J.H. Scofield, Theoretical Photoionization Cross Sections from 1 to 1500 keV, 1973. http://www.osti.gov/scitech/biblio/4545040.
[41] K. Ciosek Högström, S. Malmgren, M. Hahlin, H. Rensmo, F. Thébault, P. Johansson, K. Edström, J. Phys. Chem. C 117 (2013) 23476.
[42] L. Lombardo, S. Brutti, M.A. Navarra, S. Panero, P. Reale, J. Power Sources 227 (2013) 8.
[43] P. Walden, Z. Phys. Chem., Stoechiom. Verwandtschaftsl. 55 (1906) 207.
[44] J. Barthel, H.J. Gores, in: J.O. Besenhard (Ed.), Handbook of Battery Materials, Wiley-VCH, 1999, pp. 457–491.
[45] R. Aroca, M. Nazri, G.A. Nazri, A.J. Camargo, J. Solution Chem. 29 (2000) 1047.
[46] B. Klassen, R. Aroca, J. Phys. Chem. B 5647 (1998) 4795.
[47] S. Jeong, M. Inaba, Y. Iriyama, T. Abe, Z. Ogumi, Electrochim. Acta 47 (2002) 1975.
[48] P. Johansson, M. Edvardsson, J. Adebahr, P. Jacobsson, J. Phys. Chem. B 107 (2003) 12622.
[49] Y. Nishikawa, T. Nakano, I. Noda, Vib. Spectrosc. 49 (2009) 219.
[50] S.S. Zhang, K. Xu, T.R. Jow, J. Power Sources 113 (2003) 166.
[51] S. V Sazhin, M.K. Harrup, K.L. Gering, J. Power Sources 196 (2011) 3433.
[52] M.S. Ding, K. Xu, T.R. Jow, J. Electrochem. Soc. 149 (2002) A1489.
[53] T.-H. Nam, E.-G. Shim, J.-G. Kim, H.-S. Kim, S.-I. Moon, J. Electrochem. Soc. 154 (2007) A957.
[54] D. Aurbach, Y.S. Cohen, in: P.B. Balbuena, Y. Wang (Eds.), Lithium-ion Batteries Solid-electrolyte Interphase, Imperial College Press, 2004, pp. 70–139.
[55] M. Hellqvist Kjell, S. Malmgren, K. Ciosek, M. Behm, K. Edström, G. Lindbergh, J. Power Sources 243 (2013) 290.
[56] A.M. Andersson, M. Herstedt, A.G. Bishop, K. Edström, Electrochim. Acta 47 (2002) 1885.
[57] S. Malmgren, K. Ciosek, M. Hahlin, T. Gustafsson, M. Gorgoi, H. Rensmo, K. Edström, Electrochim. Acta 97 (2013) 23.
[58] M. Herstedt, M. Stjerndahl, A. Nytén, T. Gustafsson, H. Rensmo, H. Siegbahn, N. Ravet, M. Armand, J.O. Thomas, K. Edström, Electrochem. Solid-State Lett. 6 (2003) A202.
[59] R. Dedryvère, M. Maccario, L. Croguennec, F. Le Cras, C. Delmas, D. Gonbeau, Chem. Mater. 20 (2008) 7164.
[60] T.G. Zavalis, M. Klett, M.H. Kjell, M. Behm, R.W. Lindström, G. Lindbergh, Electrochim. Acta 110 (2013) 335.